ISAC CYTOMETRY
Journal of Quantitative Cell Science PART A

Evaluation of Caspase-3 Activity During Apoptosis with Fluorescence Lifetime-Based Cytometry Measurements and Phasor Analyses

Kapil Nichani,[1] Jianzhi Li,[1] Miho Suzuki,[2] Jessica P. Houston[1,2]*

[1]Department of Chemical & Materials Engineering, New Mexico State University, Las Cruces, New Mexico

[2]Department of Functional Materials and Science, Graduate School of Science and Engineering, Saitama University, Saitama, 338-8570, Japan

Additional Supporting Information may be found in the online version of this article.

*Correspondence to: Jessica P. Houston, Department of Chemical &Materials Engineering MSC 3805 New Mexico State University P.O. BOX 30001 Las Cruces, NM 88003 Email: jph@nmsu.edu

ISAC
INTERNATIONAL SOCIETY FOR ADVANCEMENT OF CYTOMETRY

● **Abstract**
Caspase-3 is a well-described protease with many roles that impact the fate of a cell. During apoptosis, caspase-3 acts as an executioner caspase with important proteolytic functions that lead to the final stages of programmed cell death. Owing to this key role, caspase-3 is exploited intracellularly as a target of control of apoptosis for therapeutic outcomes. Yet the activation of caspase-3 during apoptosis is challenged by other roles and functions (e.g., paracrine signaling). This brief report presents a way to track caspase-3 levels using a flow cytometer that measures excited state fluorescence lifetimes and a signal processing approach that leads to a graphical phasor-based interpretation. An established Förster resonance energy transfer (FRET) bioprobe was used for this test; the connected donor and acceptor fluorophore is cleavable by caspase-3 during apoptosis induction. With the cell-by-cell decay kinetic data and phasor analyses we generate a caspase activation trajectory, which is used to interpret activation throughout apoptosis. When lifetime-based cytometry is combined with a FRET bioprobe and phasor analyses, enzyme activation can be simplified and quantified with phase and modulation data. We envision extrapolating this approach to high content screening, and reinforce the power of phasor approaches with cytometric data. Analyses such as these can be used to cluster cells by their phase and modulation "lifetime fingerprint" when the intracellular fluorescent probe is utilized as a sensor of enzyme activity. © 2020 The Authors. *Cytometry Part A* published by Wiley Periodicals LLC on behalf of International Society for Advancement of Cytometry.

CASPASES (*c*ysteine-*asp*artic prote*ases*) are fate-determining molecules in that they are active contributors to apoptosis, inflammation, neuronal remodeling, and differentiation (1-10). Owing to the many caspases that act inside the cell, a variety of strategies can be taken to either inhibit or activate the signaling of these proteases and elicit behaviors that control cell viability. For example, identification of substrates and genetic strategies have been taken to selectively activate caspases with the goal of initiating apoptosis for cancer therapy (2-4,11-14). Despite the perceived benefits in controlling the activity of these enzymes, it remains challenging to accurately measure their function so as to determine their degree of proteolytic or nucleolytic activity (15-19).

Caspase-3, which is an effector or "executioner" caspase, has been the focus of many high content screening assays, because it is directly involved in apoptosis. Caspase-3 is mediated by initiator caspases like caspase-8. Yet, interestingly the level of caspase-3 activity is not always proportional to the extent of apoptosis in any given cell. That is, other types of paracrine signaling will regulate

caspase-3, a phenomenon recognized by situations in which protease activation levels during apoptosis remain the same despite increasing rates of acceleration of apoptotic events (20,21). Moreover, studies show that caspase-3 is involved in neural development and tissue regeneration through the control of secretion of paracrine factors (22,23), and that it mediates tumor cell growth in cells subject to radiotherapy (24). Owing to the diversity of caspase-3 function, clinical therapies that seek to control apoptotic protease functions have lagged, and additional screening approaches are sought to find reliable therapies that directly target caspases.

Toward this end, synthetic, pseudo-substrates, or "fluorogenic peptides" have been developed to detect caspase activation in vitro and report the presence of caspase families in vivo (6). Studies with multiple substrates have helped monitor localization of caspase function with attempts to explore effects by different inhibitors and activators. Yet what is lacking is quantitative knowledge about true caspase-3 activation. Caspase-3 is quite "promiscuous" in that it cleaves a variety of substrates, acts on a surprisingly diverse set of fluorogenic peptides, and acts at rates that supersede the other proteases. Ultimately, then, a single metric of "on" or "off" (i.e., cleaved or not cleaved) is insufficient (8). Added to the differences in rates of activity is the variation in the level, or amount of activated caspase-3 throughout the cell, which depends on the cell state (i.e., apoptotic, differentiating, and regenerating) (22,24-26). Therefore, it is clear that additional studies and new high throughput technologies might benefit the characterization of apoptosis through caspase-3, so as to find clinically relevant activators/inhibitors, and to identify the many circumstances under which those can affect the fate of a cell.

We have begun to address these challenges by utilizing Förster resonance energy transfer (FRET)-based bioprobes (BPs) combined with high-throughput screening approaches (27-29). With FRET-based BPs, developed by Suzuki et al., comprehensive caspase activity can be intracellularly evaluated. This is possible by connecting the donor–acceptor FRET pair with a caspase recognition sequence. When the FRET-based BP is effectively introduced into cultured cells and apoptosis is induced, caspase-3 becomes activated and available to cleave the paired donor and acceptor fluorophores, resulting in a measurable loss of FRET.

This report presents an approach to screen for this cleavage during apoptosis using a flow cytometer that measures fluorescence lifetimes. The fluorescence lifetimes of the donor molecule during and after FRET is measured and interpreted in order to observe changes, cell-by-cell. Our approach involves frequency-domain cytometry analyses that culminate with a phasor representation of the activation of caspase-3 activity throughout large cell populations. Future outcomes of this high-throughput approach may include the ability to quantitatively measure caspase-3 activity after induction of apoptosis and when modulating cell populations with protease inhibitors.

THEORY AND PRAXIS

In order to establish a quantitative approach for measuring caspase activity, a variety of FRET bioprobes were developed and evaluated for functionality (27-29). The purpose of these BPs was to evaluate enzyme activation and identify caspase activity with precision owing to the specificity of the engineered cleavage peptide sequence (27-29). We have selected for this study an optimized and reproducible BP in order to evaluate our ability to measure the changes in the donor lifetime using time-resolved flow cytometry. Our goal is to turn average lifetime data from single cells into statistically relevant information that assesses the heterogeneity in caspase-3 activation and patterns cell populations follow as they experience loss of FRET.

FRET, a nonradiative dipole–dipole interaction process, has been widely used as an "optical ruler" to identify the spatial and temporal function of many biological and intracellular events and mechanisms (30). As an optical tool, FRET can be exploited in order to evaluate interactions between molecules. That is, when FRET-dependent optical signals are measured, the spectral data can be used to calculate Förster distances and thereby infer distances between molecules linked to the donor and acceptor (31-33). FRET parameters can be determined with flow cytometry by measuring either a decrease in the donor fluorescence, sensitized emission of the acceptor (34), or changes in the fluorescence lifetime of the donor (35). It is most accurate when all three photophysical characteristics are collected (27-30).

We have developed a variety of cytometry systems to measure fluorescence lifetimes (35-39). These approaches are generally referred to as time-resolved flow cytometry (TRFC). In this contribution, we apply TRFC to a FRET pair using green fluorescence protein (GFP) as the donor fluorophore and Alexa Fluor® 546 dye (Thermo Fisher Scientific, Waltham, MA) as the acceptor molecule. The pair is connected with a caspase-3 peptide recognition sequence (Förster distance = 10.5 nm) (27-29,40) and frequency-domain TRFC analyses are performed.

FRET, when determined using fluorescence lifetime measurements, is favorable because the fluorescence decay kinetics of the donor fluorophore are independent of concentration and artifacts that affect fluorescence intensity (41-43). The fluorescence lifetime leads to a direct evaluation of FRET efficiency requiring less experimental controls, extensive calibration, and normalization procedures. In general, fluorescence lifetimes are independent of the amount of fluorophore inside the cell when no aggregation or self-quenching is present. Moreover, in situations where spectral overlap challenges the ability to resolve an optical signal (i.e., presence of two or more unique fluorophores expressed intracellularly with similar emission spectra), the measurement of fluorescence lifetimes can aid in the evaluation of the amount of each fluorophore present. Lifetime analyses are also independent of excitation intensity and exposure duration, which does affect intensity-based measurements.

With the TRFC described herein, the fluorescence lifetime is collected as an average, representing the average time all fluorophores inside the cell remain in the excited state prior to decaying to their ground state through emission of photons. The fluorescence lifetime, denoted by the symbol, τ, can be measured using cytometry systems that are configured to excite samples with pulsed lasers (time-domain), radio-frequency modulated lasers (i.e., frequency-domain), or even with conventional systems as we have shown in the past (44). In this work we use a modified frequency-domain flow cytometer (see schematic, Fig. 1) and collect cytometric waveforms that include modulated side-scattered light signals and modulated fluorescence signals from each cell where these correlated signals are used to compare the fluorescence lifetime cell-by-cell. With signal processing, the modulated signals can be evaluated in ways that allow us to extract both the fluorescence phase lifetime and modulation lifetime, which are parameters that are associated with the decay kinetics within each cell. Mathematically these lifetimes are represented by

$$\tau_\phi = \frac{tan(\phi)}{\omega}, \quad \text{and} \tag{1}$$

$$\tau_m = \frac{1}{\omega}\sqrt{\frac{1}{m^2} - 1} \tag{2}$$

where τ_ϕ and τ_m are phase and demodulation lifetimes, respectively, ϕ is the phase rotation between excitation and emission signals, ω is the frequency of modulation, and m is the demodulation depth. In the evaluation herein, we use the fluorescence lifetime to compute a semi-quantitative FRET efficiency parameter (E_{FRET}) by the equation below:

$$E_{\text{FRET}} = 1 - \frac{\tau_{\text{DA}}}{\tau_{\text{D}}} \tag{3}$$

where τ_{DA} is the fluorescence lifetime of the donor in presence of acceptor and τ_{D} is the lifetime of the donor-only molecule. If the cleavage of the BPs is a direct outcome of the action of caspase-3, a measurement of E_{FRET} can aid in characterizing activation of the enzyme within the cell before and after apoptosis induction.
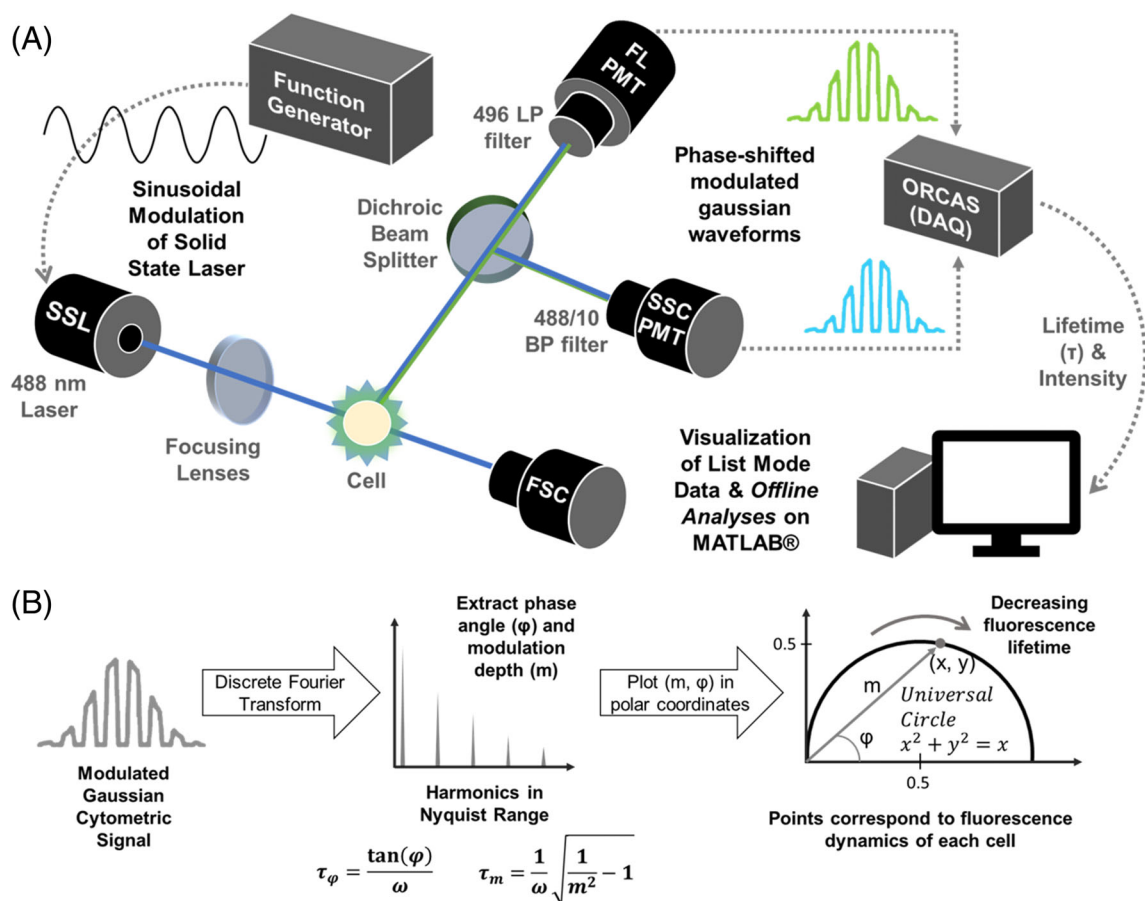
Fig 1. Illustrations of time-resolved flow cytometry instrumentation and analysis schema. (**A**) A diagram of a simple flow cytometer constructed for the measurement of FRET. (**B**) The procedural steps to evaluate FRET data using phasor analyses. [Color figure can be viewed at wileyonlinelibrary.com]

Phasor Analysis

In addition to standard lifetime analyses, a phasor representation of the FRET bioprobe can be evaluated. Phasor plots are visualization graphs developed for fluorescence lifetime imaging microscopy (FLIM) to better characterize population-wide changes. We have demonstrated how phasor graphing can be adapted to flow cytometry, which is an approach analogous to the FLIM phasors (44) yet distinct in how data are obtained and processed (see Table 1 for a comparison). In cytometry, phasor analyses are quite powerful as graphical tools because phasor plot information leads to inferences about discrete FRET states and the ability to compute the fraction of acceptor-bound donor molecules on a single cell basis.

In this work, we establish an approach that leads to a phasor analysis of the caspase-3 FRET BP. This is accomplished by transforming cytometric waveforms collected with a TRFC into Fourier space to obtain cell-to-cell frequency spectra. From the spectra, the phase and amplitude at each harmonic are extracted to evaluate the phase lifetime (τ_ϕ) and demodulation lifetime (τ_m). A phasor graph is established by a coordinate transformation of these values so that they can be plotted, where each point is representative of the two values from each cell. Additionally, an outer semicircle (i.e., the "universal circle") is graphed to represent the single exponential decay boundary. Figure 1 depicts the procedural steps to generate a cytometry-derived phasor plot.

Table 1. Comparison of phasor analyses using FLIM and lifetime-cytometry

	FLOW CYTOMETRY	MICROSCOPY
Phasor development based on instrument features (44–47)		
Excitation signal	Frequency domain: modulated laser with width in 100s of μm thus larger than cell passing through.	Frequency or time domain: laser spot diameter smaller than cell, higher fluence and scanned, repetitively.
Emission signal	1 to 10 μs: amount of time cell passes through focused laser beam; only one measurement per cell.	100s of ms: amount of time camera is integrated during a FLIM measurement; repeated integrations of each cell are possible.
Phasor data and analysis (48–50)		
Numbers of cells	Large numbers of cells (1,000's) are investigated passing through the laser beam.	Fewer cells are studied (10s or 100s), depending on the magnification and field of view.
Photon counts	Large spread of points = heterogeneity of cell population and distribution of fluorescence decay properties across the entire cell population.	Large spread of points = higher noise in pixel values, and low photo economy.
Image construction	Data points result from Fourier transform of waveforms correspond to each cell; resulting point cloud represents entire cell population.	Data points result from intensity stack of images (homodyne frequency domain, time gated, or time-correlated single photon count); resulting point cloud represents a pixel population.
Application and utility (35,39,46,51–55)		
Sorting and segmentation	Cell populations on phasor plot can be gated and the signals can be triggered to sort cell samples.	Pixel population can be gated and used to classify or segment different regions within a cell.
Spatial dimension	Adds a spatial dimension to visualize, and gate cell populations.	Global analysis of fluorescence decay kinetics, circumventing fitting processes, but nondiscriminatory in term of spatial position in the cell.
FRET studies	Superimposed data for quenched donor and partially quenched donor leads to dequenching trajectories to track cell populations undergoing loss of FRET.	Superimposed data for quenched donor, background autofluorescence and dequenched donor leads to a FRET trajectory to study FRET efficiencies.
Fingerprinting	The phasor for a mixture of fluorescence species can be decoupled to obtain the molecular fraction of its constituents in the phasor space. This is possible as the mixture is a linear combination of the phasors of its constituents.	
Characteristics of decay kinetics	Sample exhibiting single exponential decay kinetics are positioned on the semicircle, whereas multiexponential decay kinetics fall inside the circle, and photochemical reactions fall outside the semicircle.	

Materials and Methods

Extraction and Purification of Green Fluorescent Protein as the FRET Donor

In order to develop a FRET-based BP we followed Suzuki et al. (27-29) and expressed and purified a modified, or "mutant," green fluorescent protein (GFP-μ) by insertion of a caspase-3 cleavable short peptide sequence (DEVD). Briefly, the procedure involves transforming plasmids into competent *Escherichia coli* (BL-21 DE3, Invitrogen by Life Technologies, Carlsbad, CA). *E. coli* were cultured (37°C), harvested, and lysed. The lysate was separated and purified (column with Ni^{2+} − NTA resin, Thermo Fisher Scientific Inc., Waltham, MA), as per standard procedures with histidine tagged fusion proteins. GFP-μ was recovered after purification and reconstituted in phosphate-buffered saline and checked for purity spectroscopically (i.e., ratio of absorbance at 488 and 280 nm > 1.5).

Construction of the Bioprobe

The acceptor molecule used was an organic fluorophore, Alexa Fluor® 546 dye (Thermo Fisher Scientific Inc.) with an excitation maximum that sufficiently overlaps with the emission spectrum of GFP-μ (27-29,56,57). This fluorophore also has a quantum yield that is high relative to other Cy3 derivatives with similar emission profiles. Alexa Fluor® 546 dye was conjugated to GFP-μ by reduction of the disulfide bonds of the protein with dithiothreitol (DTT); 100 μl of a 20 μM protein solution was reduced with 1 mM DTT at room temperature for 15 min. Excess DTT was removed using Zeba™ spin desalting columns (Thermo Fisher Scientific Inc.). Alexa Fluor® 546 dye dissolved in dimethyl sulfoxide (DMSO) (concentration estimated spectrophotometrically using extinction coefficient at 554 nm, $e_{554} = 106{,}000$ cm^{-1}M^{-1}) was mixed with GFP-μ with a GFP-μ/Alexa Fluor® 546 dye at a ratio of 1:10. The mixture was incubated for 4 h at 37°C. Excess Alexa Fluor® 546 dye was removed using Zeba™ spin desalting columns. The final FRET bioprobe is referred to as GFP-μ-A546 from here forward.

Caspase-3 Cleavage Test

The GFP-μ-A546 BP was tested in vitro for cleavage by combining with two units of caspase-3 (EMD Millipore, Bedford, MA). The solution (5 μM) was reconstituted in a buffer with 20 mM 2-[4-(2-sulfoethyl) piperazin-1-ium-1-yl] ethanesulfonate (PIPES), 100 mM NaCl, 0.1% 3-[dimethyl (3-([(3α,5β,7α,12α)-3,7,12-trihydroxy-24-oxocholan-24-yl] amino)propyl)ammonio]propane-1-sulfonate (CHAPS), 10 mM DTT, 10% sucrose, and 1 mM EDTA. This mixture was incubated at 30°C for 2-, 5- and 7-h to evaluate caspase-3 cleavage response time. Cleavage was evaluated by measuring total fluorescence emission spectra (with a Horiba FluoroMax®-4 spectrofluorimeter).

Cell Culture

HeLa cells (ATCC.org®) were cultured as this line is known to have a strong caspase-3 expression when apoptosis is induced with tumor necrosis factor-α (TNF-α) and cycloheximide (CHX). In preparation for the evaluation of FRET, cells were cultured in a humidified atmosphere at 37°C and 5% CO$_2$. Cells were cultured in Dulbecco's modified Eagle's medium (DMEM) with 10% fetal bovine serum (FBS) in T-25 flasks and six well plates. In preparation to add the GFP-μ-A546 to the cells, 50 μl (∼25 μM) of the BP was added to a lyophilized film of BioPORTER reagent (Genlantis, San Diego, CA) and incubated at room temperature for approximately 10 min to insure hydration of the dry-film and formation of BioPORTER protein complexes. DMEM without FBS was also added so the resulting solution could be combined with the monolayer HeLa cells. The solution was added to cells cultured to 80 to 90% confluency. The same procedure was followed for the control in which the donor-only mutant GFP molecule was introduced into HeLa cells. After a 3-h incubation, the cells were washed, detached (0.25% Trypsin, Life technologies, Grand Island, NY), centrifuged, and resuspended in phosphate buffered saline to obtain volumes at a concentration of approximately 10^6 cells/ml to be used for cytometry experiments.

Apoptosis Evaluation with Annexin V and Propidium Iodide (PI)

The evaluation of apoptosis induction in cells was with a standard annexin-PI cytometry assay. Aliquots of HeLa cells were treated with apoptosis-triggering reagents, TNF-α and CHX. After different time points, HeLa cells were collected and labeled with an annexin V fluorophore and PI. This procedure involved taking resuspended cells and combining with a 1× binding buffer containing 5 μl fluorescein 5-isothiocyanate [FITC; 2-(3,6-dihydroxy-9H-xanthen-9-yl)-5-isothiocyanatobenzoic acid] following the manufacturer's protocol for annexin V detection (BD Biosciences, Franklin Lakes, NJ). Additionally, 2 μl of propidium iodide was added to the cell suspension and mixed gently for live/dead cell analysis. The cells were evaluated using a BD Accuri™ C6 flow cytometer (BD Biosciences) to collect fluorescence intensity of FITC-annexin V and PI as well as forward scatter and side scatter values.

Cytometric Evaluation of the BP Before and During Apoptosis

Experimentally, we measured cells with GFP-μ-A546 before apoptosis induction and after apoptosis induction at different time points as well as cells with only GFP-μ. Our evaluation involved measuring changes in the fluorescence intensity and fluorescence lifetime of the donor fluorophore.

A BD Accuri™ flow cytometer was used to evaluate donor emission and acceptor emission in a qualitative manner with the goal of evaluating GFP-μ and GFP-μ-A546 internalization within the cells. We thus collected optical signals at the peak emission of the donor molecule as well as the acceptor molecule (530/15 and 585/20-nm, when excited at 488-nm). A preliminary estimation of sensitized acceptor emission was performed with these data by taking the "FRET ratio" using the mean fluorescence intensity (MFI) of cells

measured at the acceptor channel, divided by the MFI of the donor channel. This type of FRET ratio is an observational metric only because full FRET assessment requires additional intensity-based FRET controls, as reported by Nagy et al. (34) and others (58).

The time-resolved cytometry measurements were performed with a retrofitted BD FACSVantage™ SE (BD Biosciences) cell sorter (Fig. 1). A 488-nm, 50 mW solid-state diode laser (Coherent Inc. OBIS, Santa Clara, CA) was used and digitally modulated at a sinusoidal radio frequency of 6.25 MHz (Tektronix AFG-3102 arbitrary function generator, Beaverton, OR). Side scattered light (SSC) was collected through a 488/10 nm band pass filter into a photomultiplier tube (PMT) detector (model: R1477-04, Hamamatsu Photonics, Lake Forest, CA). Fluorescence emission of the donor was detected using a 496 nm long pass filter and similar PMT detector. Signals from the PMTs were amplified (60 dB, AC-100, Advanced Research Instruments Corp., Bandon, OR) and digitized at 50 mega samples per second. Full cytometric waveforms were collected as were standard .fcs files which include the average fluorescence lifetime per cell as a parameter. Calibration with a known fluorescence lifetime is required for TRFC, which was achieved using Flow-Check™ fluorospheres (Beckman Coulter, CA), which have lifetimes reported to be 7 ns (59). After calibration, all settings remained constant for proceeding experiments.

RESULTS AND DISCUSSION

Bioprobe Characterization and In-Vitro Caspase-3 Digestion

To first evaluate the cleavage of the GFP-μ-A546, we performed an in vitro evaluation with spectrofluorimetry. Fluorescence intensities were evaluated in which we analyzed the brightness levels across both the emission spectrum of the donor and acceptor fluorophores. This cleavage of the BP in vitro (schema depicted by Fig. 2) was determined in solution. Spectrofluorimetry results (Supplementary Fig. S1) can be visualized by the normalized spectra with acceptor fluorescence shifting upon introduction of the caspase-3. On calculating the ratio of fluorescence intensities corresponding to acceptor and donor fluorophores (I_A/I_D), values of 0.94 and 0.66 were determined in the absence and presence of caspase-3 (digested for 7 h), respectively. These results also confirm prior work (27-29).

Apoptosis Optimization with Annexin-V and PI

We selected time points to observe apoptosis post-treatment based on the results from an annexin V–PI apoptosis assay (60). The cytometry data (see Supplementary Fig. S2) indicate apoptosis by an increase in PI and annexin V-(FITC) at the onset of apoptosis as compared to non-apoptotic cells. Initially apoptosing doses of 40 ng/ml TNF-α and 100 μg/ml CHX were used to find a percentage of total cells increasing in the FITC channel from 21% after 2 h to 52 and 78% after 6 and 12 h of treatment, respectively. The percentage of total cells increased in the PI channel from 17% after 2 h to 37 and
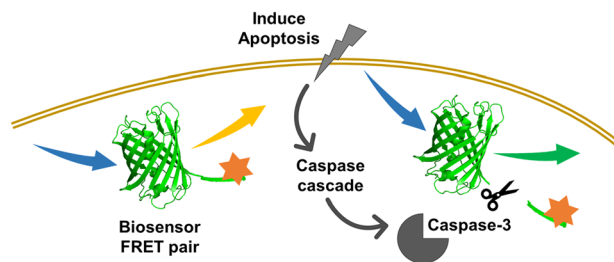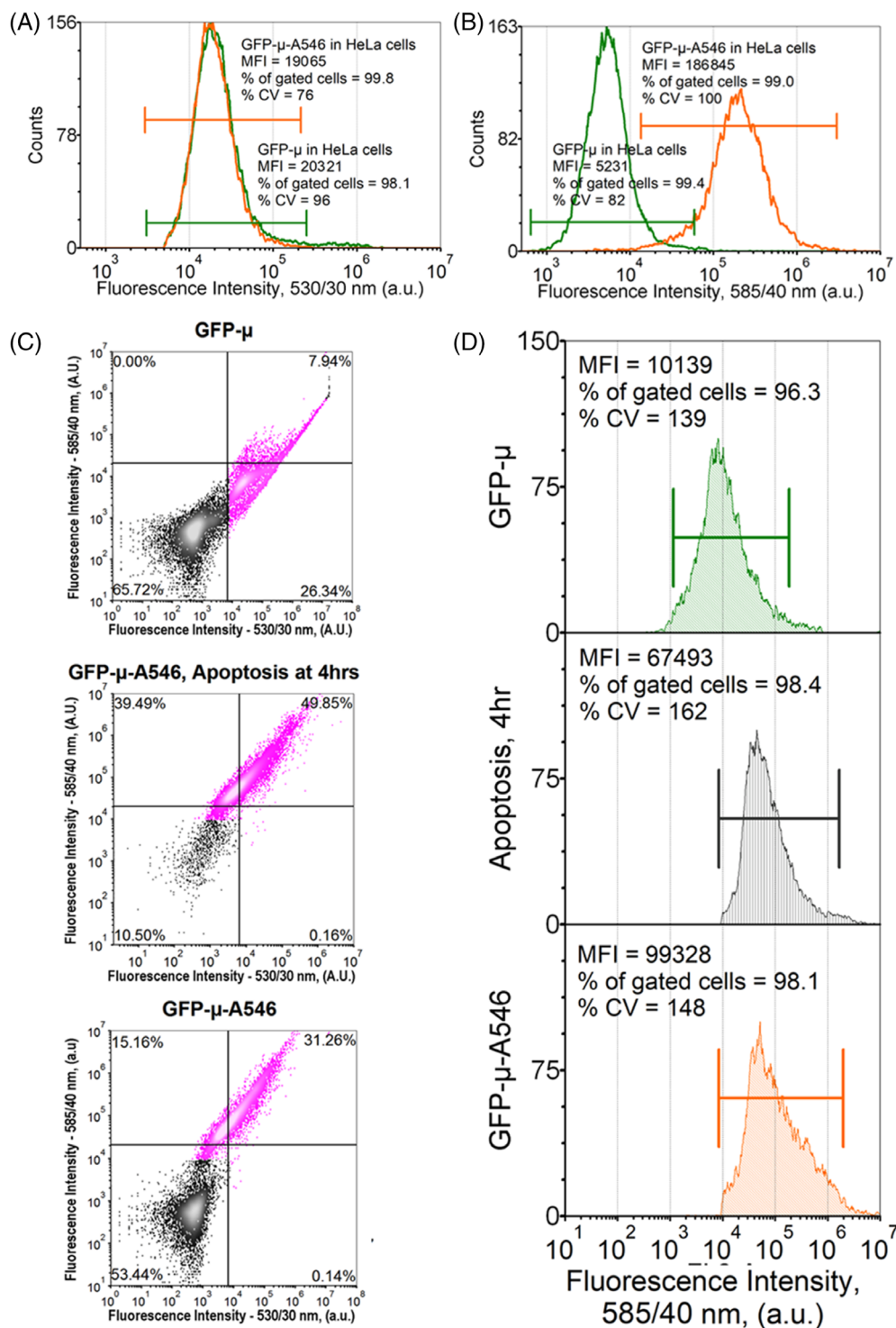

Fig 2. Illustration of a cell depicting external apoptosis induction (lipid bi-layer depicted by double lines) and the resulting intracellular caspase activation. The bioprobe is introduced into the cell as a FRET pair connected by a caspase-3 recognition sequence. When apoptosis is induced, the FRET pair is cleaved by active caspase-3. Before as well as after cleavage, fluorescence emission is measured in both donor and acceptor channels; additionally, the fluorescence lifetime is measured from the donor emission. [Color figure can be viewed at wileyonlinelibrary.com]

72%, after 6 and 12 h of treatment, respectively. A range of concentrations were evaluated to find these optimal conditions (e.g., higher doses tested: 80 ng/ml TNF-α and 200 μg/ml CHX) but resulted in higher cell death percentages. Thus, 40 ng/ml TNF-α and 100 μg/ml CHX was selected for apoptosis assessment between a 2- to 6-h time point.

Analysis of the FRET BP with Cytometry

The fullest evaluation of FRET should involve a number of important controls, and evidence of FRET is typically determined by evaluating FRET efficiencies. Some of these methods involve determination of cross-FRET, implementing "dark GFP" with the acceptor attached, 1:1 donor-acceptor pairs with "zero efficiency," bleed-through evaluation, acceptor photobleaching, detection of fluorescence emission levels for autofluorescence, as well as measuring GFP-μ-A546, and GFP-μ when excited at both donor acceptor wavelengths (32,34,42). In this work, we use cytometry measurements as a semiquantitative estimate with a simple scenario in which the populations of cells are screened for sensitized emission of the acceptor fluorophore when compared to donor-only cells. This approach is taken to set the stage for lifetime and phasor approaches, performed with TRFC data and signal processing.

Shown in Figure 3A,B are cell counts when observing emission at the donor and acceptor channels. Figure 3A interestingly suggests that cells that have GFP-μ-A546 have a mean donor emission that is not significantly lower than cells with GFP-μ only. This similarity was found to be reproducible and is attributed to a number of factors, which include unwanted residual and unbound donor GFP-μ in cells that contain GFP-μ-A546, different fluorescent dye modification efficiencies (60% or more might occur), and different uptake of the fluorophore and BP for different cell populations. When measuring sensitized acceptor emission (Fig. 3B) the cells with GFP-μ-A546 had expectedly higher levels than cells with only GFP-μ (low, or no acceptor emission).

Caspase-3 in Fluorescence Lifetime-Based Cytometry Measurements and Phasor Analyses
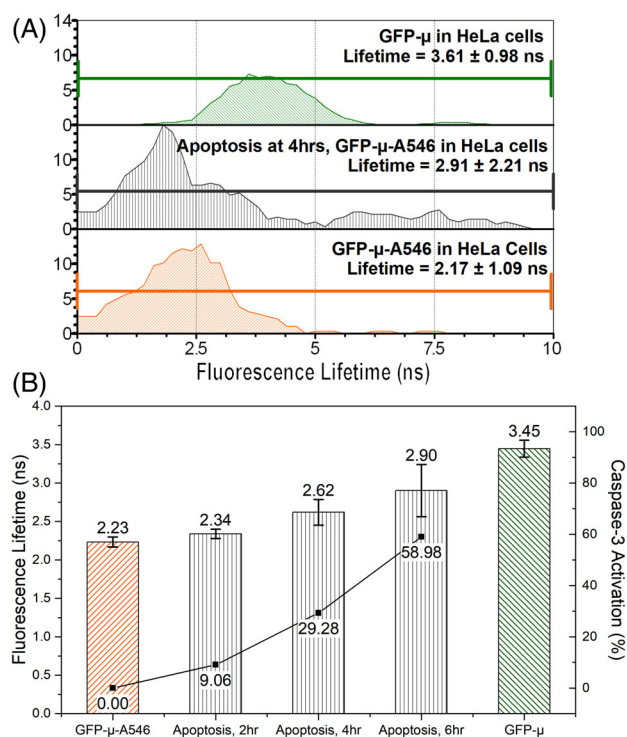
Fig 3. Flow cytometry measurement results including fluorescence emission at both donor and acceptor emission peak channels. Panels **A** and **B** include data from cells with the GFP-µ-A546 BP and GFP-µ only. Panel **C** includes bivariate histograms of the donor versus the acceptor channel and include unlabeled cells overlays for background reference. The top graph of panel C includes cells with GFP-µ only, followed by GFP-µ-A546 BP when apoptosis is induced (middle) and not induced (bottom). Panel **D** include the corresponding histograms of acceptor emission channel, which aid in assessment of BP presence intracellularly when screening for sensitized acceptor emission. [Color figure can be viewed at wileyonlinelibrary.com]

Figure 3C includes cytometry results represented as the donor versus acceptor emission channel to estimate total cell counts for cells expressing a nominal level of intracellular GFP-μ-A546 in comparison to cell counts with populations in which the GFP-μ-A546 BP is affected by induction of apoptosis. Additionally, Figure 3C includes cell population data for cells expressing only the GFP-μ emission. These data also include unlabeled cells. The cell populations with only GFP-μ were not measured during apoptosis, whereas slight to large GFP emission signal changes can occur owing to changes within intracellular micro-environments (metabolic, pH, cell proliferation, cell death, etc.). Figure 3C cannot fully predict FRET but does aid in tracking the percentage of cells that have changes in sensitized acceptor emission during apoptosis. For example, the increase in acceptor positive percentages during apoptosis (Fig. 3C, middle vs. lower graph) is obvious when controlling for only apoptosis induction within the same cell population. We also assessed sensitized emission using the FRET ratio (shown in Supplementary data Fig. S3), which is also an informative estimate to compare cells with GFP-μ-A546 before and during apoptosis, albeit with a nonquantitative FRET approach. A full FRET experiment (going beyond the scope of this short report) requires an arduous protocol, mandating donor-only and acceptor-only samples excited separately for FRET efficiency calibrations because of the possibility of acceptor cross-talk in the donor channel. Our cytometry system lacks the required optical platform that is commensurate of FLIM-FRET, which requires dual excitation and detection for simultaneous and/or sequential measurements across all required spectral emission channels.

Additional changes in the percentages of cells when measuring sensitized acceptor emission are displayed by Figure 3D. These include before and during apoptosis as well as for cells only expressing GFP-μ. The MFI for cells that should not be experiencing sensitized emission is ∼10× lower than cells with the intracellular GFP-μ-A546. Also, cells with GFP-μ-A546 had an MFI (acceptor channel) that dropped by 30% after 4 h under apoptosis. These data were reproducible (population: $n = 3$), allowing us to verify the presence of GFP-μ-A546 within the cells and changes thereof during apoptosis.

It is worth noting that the cytometry intensity data from Figure 3 is not a holistic assessment of FRET and is moreover influenced by a range of factors such as a loss of cells owing to apoptosis (i.e., increase in dead cells and debris) and a variability owing to differences in the amount of GFP-μ-A546 uptake into cells. In this report, we include these graphs to show how linear trending data can be used to identify a changing slope, which suggests a dependence on FRET efficiency. Thus, we emphasize that the fundamental result is that the overall emission on induction of apoptosis in the acceptor emission channel decreases to levels lower than the brightest FRET signal and higher than the brightest non-FRET signal (i.e., donor only). We also note that a full FRET interpretation with standard cytometry was evaluated and presented in prior work (27-29). These intensity data simply allow us to recognize an expected trend, permitting the advancement to TRFC measurements.

Evaluation of the Cleavage of the FRET BP with TRFC

Figure 4 are data from TRFC in which we found the average fluorescence lifetime (Fig. 4A) of GFP-μ, to be similar to that of reported literature values (e.g., 3.1–3.3 ns) (40,61). Additionally, cells that have GFP-μ-A546 before apoptosis have an average donor fluorescence lifetime of 2.17 ns and cells measured after 4 h of induction of apoptosis had a fluorescence lifetime of 2.91 ns. These values are average fluorescence lifetimes per-cell, and the reported values are means of each cell population. The cleavage of the FRET BP by caspase-3 activation initiates a lengthening of the donor fluorescence lifetime, which we detect by TRFC. Interestingly the distributions are large with events that fall across a long lifetime range (>3 ns). We have included these lifetime "tails" in the mean calculation (notice markers in Fig. 4A include all cells) to avoid a biased assessment. The wide lifetime distributions are a product of TRFC system limitations and measurement noise. For example, there are inherently low photon counts when

Fig 4. Data of fluorescence lifetime values during caspase-3 activity measured by time-resolved cytometry. (**A**) Fluorescence lifetime histograms of counted cells with GFP-μ-A546 before and after apoptosis as well as cells with GFP-μ only. (**B**) Compares the mean fluorescence lifetimes obtained across 3 repeat measurements for apoptosing cell populations over 2, 4, and 6 h post-treatment with the TNF-α and CHX inducing reagent. Error bars are representative of the standard deviation of the mean fluorescence lifetimes. Also shown are data of the average percent caspase-3 activity through a line plot over the fluorescence lifetime bar graphs. [Color figure can be viewed at wileyonlinelibrary.com]

collecting donor emission signals at rapid cell transit times. Additionally, our instrumentation has an upper limit to the laser modulation frequency owing to low data acquisition sampling rates (i.e., Nyquist = 25 MHz). Despite these TRFC challenges, we were able to detect reproducible lifetime shifts for repeated, independent experiments, and note that the data processing included gating and thresholding schemas to ensure that single, bright cells are counted.

Figure 4B compares the mean fluorescence lifetimes obtained across 3 repeat measurements for apoptotic cell populations over 2, 4, and 6 h post-treatment with the TNF-α and CHX inducing reagent. Error bars are representative of the standard deviation of the mean fluorescence lifetimes. The increasing trend suggests that the fluorescence lifetimes of the donor are becoming similar to the donor-only fluorescence lifetime. Also shown in Figure 4B is an estimation of the relative caspase-3 activation. The caspase-3 activation across each cell population was calculated using the relative difference in the FRET efficiency parameter (E_{FRET}) and added as a line plot to the fluorescence lifetime bar graphs for a correlative perspective.

The phase and demodulation lifetimes are presented in Figure 5 as phasor graphs both in illustrative form (Fig. 5A) and of real TRFC data (Fig. 5B). As described previously, the modulated cytometric signals measured for each stage before and after apoptosis were collected per cell. These "cytometric waveforms" from the fluorescence and side-scatter channels were digitized and processed to evaluate the demodulation and phase shift values using a Fourier transformation. With polar coordinates, the phase and demodulation are plotted where each point on the phasor graph represents the two values from one cell.

Figure 5A first illustrates the concept of a phasor graph and what can be expected when the median of the population of cells changes owing to the induction of apoptosis. This is viewed as a trajectory, or "map" that can be taken by the populations before and after cleavage. For example, a population of cells with the donor not in the presence of the acceptor (GFP-μ only, green dot) would result in a single-lifetime, largest-phase, and high demodulation value (upper left portion of the phasor). Cells with the donor in the presence of the acceptor (GFP-μ-A546, orange dot) have a lower angle in phase and demodulation depth, resulting in a new location in the center of the phasor graph that represents the "uncleaved" (i.e., 0% caspase activation) position. This position is typically found on the outer right periphery of the semicircle when measured by FLIM (62). Cytometry systems track cells in motion (as opposed to long FLIM interrogation times) and are thus challenged by low donor emission signals, which can influence the phasor position (35). Lastly, cells undergoing apoptosis (gray dot) will show a higher positional location on the phasor because they contain the cleaved GFP-μ-A546 BP (i.e., degree of phase is larger). The location of the points on the graph is visual aids for mapping the trajectory during this process.

Figure 5B includes data from cells to observe the pattern when apoptosis is induced. The density contours guide the viewer to where regions of cells are most alike. Plotted are two cell groups: cells with GFP-μ-A546 BP before apoptosis and cells with GFP-μ-A546 BP during apoptosis. The phasor is used to observe the distribution of cells with GFP-μ-A546 prior to caspase-3 activation (leftmost group and inner phasor) and compare this to cells during activation (rightmost groups). Interestingly during activation, there are two dominant populations: (1) a population where the phase is similar to the non-activated cells but the demodulation is higher (right, lower periphery–donor lifetime remains shortened but brighter signals are detectable) and (2) a population where the phase is high as well as the amplitude demodulation (phase increases and amplitude demodulation remains high). These positions on the phasor help to understand what cells have experienced caspase-3 at different activated levels (i.e., secondary group experienced more cleavage) and thus map the activity of the enzyme dynamically. Although the TRFC system we use is challenged by the modulation frequency limits as well as the presence of low donor emission
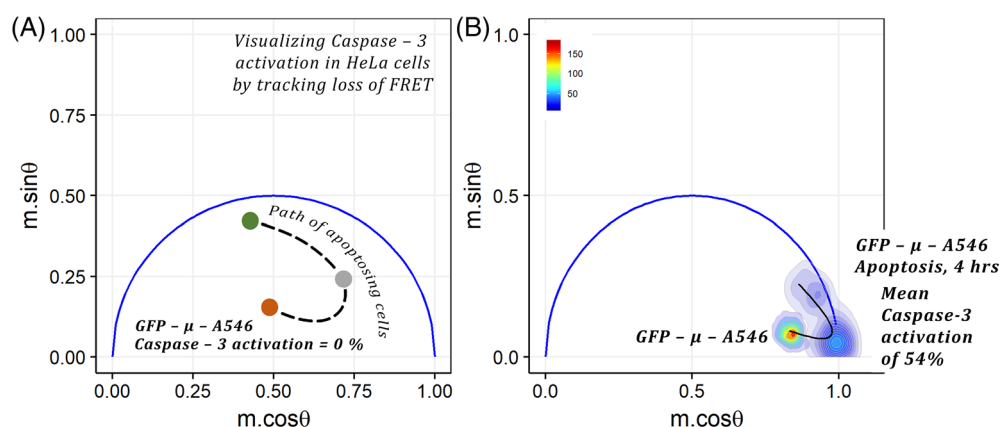
Fig 5. Phasor graphs both in illustrative form (**A**) and of real time-resolved cytometry data collected (**B**). (A) Diagrams the concept of a phasor graph and what can be expected when the median of the population of cells changes owing to the induction of apoptosis. (B) Data of cells with the FRET BP before apoptosis and during apoptosis (4 h) with the caspase activation trajectory interpretation. [Color figure can be viewed at wileyonlinelibrary.com]

signals, which both impact the lifetime resolution, we are able to interpolate between the mean of each population to generate a trajectory of activation. In future work, with an improved TRFC sensitivity that includes autofluorescence lifetimes, we can quantify full FRET and thus the impact of compounds against molecular targets of apoptosis. Finally, we plan to use the phasor graph to gate cells at different stages of the trajectory and sort those with different levels of FRET efficiencies for further evaluation.

CONCLUSION

Caspases are targets for strategies that inhibit or activate apoptosis, and such strategies might range from initiation of substrates to genetic approaches that are beneficial for biomedical applications such as cancer therapy. Yet despite the evident role of caspase-related enzymatic activity during apoptosis, there is a consensus that tracking apoptosis with a single endpoint determination is not entirely accurate. This inaccuracy is partly because of the ambivalent nature of the commitment of various caspases to diverse versions of programmed cell death such as apoptosis, necroptosis, pyroptosis, oncoptosis, and autophagy; their lethal functions are attributed to evolution whereas some non-lethal functions are phylogenetically conserved (63,64). Owing to studies such as these, we share in this report a screening approach that is dynamic in the sense that caspase activity can be mapped at different stages by exploiting a FRET-based BP and estimating a caspase activation trajectory. This approach builds on prior average fluorescence lifetime estimates and demonstrates a cytometry-based phasor methodology. Our goal is to assist in the tracking of caspase-3 activation levels during apoptosis and set the stage for future quantification of enzyme activity using a range of BPs. Further work also may include sorting events based on relative phasor positioning thus enabling the isolation of cells across any continuum of caspase activation. With this tool, cells can be further evaluated for very subtle differences in signal transduction as a result of different triggering reagents.

AUTHOR CONTRIBUTIONS

Kapil Nichani: Data curation; formal analysis; investigation; methodology; writing-original draft. **Jianzhi Li:** Data curation. **Miho Suzuki:** Conceptualization; formal analysis; methodology. **Jessica Houston:** Conceptualization; project administration; resources; supervision; writing-review and editing.

LITERATURE CITED

1. Yuan J, Kroemer G. Alternative cell death mechanisms in development and beyond. Genes Dev 2010;24:2592–2602.
2. Shi Y. Mechanisms of caspase activation and inhibition during apoptosis. Mol Cell 2002;9:459–470.
3. Alnemri ES, Livingston DJ, Nicholson DW, Salvesen G, Thornberry NA, Wong WW, Yuan J. Human ICE/CED-3 protease nomenclature. Cell 1996;87:171.
4. Fiandalo MV, Kyprianou N. Caspase control: Protagonists of cancer cell apoptosis. Exp Oncol 2012;34:165–175.
5. Salvesen GS, Hempel A, Coll NS. Protease signaling in animal and plant-regulated cell death. FEBS J 2016;283:2577–2598.
6. Poreba M, Strózyk A, Salvesen GS, Drag M. Caspase substrates and inhibitors. Cold Spring Harb Perspect Biol 2013;5:a008680.
7. Denault JB, Salvesen GS. Apoptotic caspase activation and activity. Methods Mol Biol 2008;414:191–220.
8. McStay GP, Salvesen GS, Green DR. Overlapping cleavage motif selectivity of caspases: Implications for analysis of apoptotic pathways. Cell Death Differ 2008;15:322–331.
9. Salvesen GS, Riedl SJ. Caspase mechanisms. Adv Exp Med Biol 2008;615:13–23.
10. Stennicke HR, Salvesen GS. Properties of the caspases. Biochim Biophys Acta 1998;1387:17–31.
11. Shariat SF, Desai S, Song W, Khan T, Zhao J, Nguyen C, Foster BA, Greenberg N, Spencer DM, Slawin KM. Adenovirus-mediated transfer of inducible caspases: A novel "death switch" gene therapeutic approach to prostate cancer. Cancer Res 2001;61:2562–2571.
12. Hensley P, Mishra M, Kyprianou N. Targeting caspases in cancer therapeutics. Biol Chem 2013;394:831–843.
13. Morgan CW, Julien O, Unger EK, Shah NM, Wells JA. Turning on caspases with genetics and small molecules. Methods Enzymol 2014;544:179–213.
14. Favaloro B, Allocati N, Graziano V, Di Ilio C, De Laurenzi V. Role of apoptosis in disease. Aging (Albany NY) 2012;4:330–349.
15. Cho DH, Jo YK, Hwang JJ, Lee YM, Roh SA, Kim JC. Caspase-mediated cleavage of ATG6/Beclin-1 links apoptosis to autophagy in HeLa cells. Cancer Lett 2009;274:95–100.
16. Zhu C, Wang X, Hagberg H, Blomgren K. Correlation between caspase-3 activation and three different markers of DNA damage in neonatal cerebral hypoxia-ischemia. J Neurochem 2000;75:819–829.
17. Zhu Y, Ahlemeyer B, Bauerbach E, Krieglstein J. TGF-beta1 inhibits caspase-3 activation and neuronal apoptosis in rat hippocampal cultures. Neurochem Int 2001;38:227–235.
18. Fan W, Dai Y, Xu H, Zhu X, Cai P, Wang L, Sun C, Hu C, Zheng P, Zhao BQ. Caspase-3 modulates regenerative response after stroke. Stem Cells 2014;32:473–486.
19. Zhu HC, Gao XQ, Xing Y, Sun SG, Li HG, Wang YF. Inhibition of caspase-3 activation and apoptosis is involved in 3-nitropropionic acid-induced ischemic tolerance to transient focal cerebral ischemia in rats. J Mol Neurosci 2004;24:299–305.
20. Shalini S, Dorstyn L, Dawar S, Kumar S. Old, new and emerging functions of caspases. Cell Death Differ 2015;22:526–539.
21. Denton D, Nicolson S, Kumar S. Cell death by autophagy: Facts and apparent artefacts. Cell Death Differ 2012;19:87–95.
22. Li F, Huang Q, Chen J, Peng Y, Roop DR, Bedford JS, Li CY. Apoptotic cells activate the "phoenix rising" pathway to promote wound healing and tissue regeneration. Sci Signal 2010;3:ra13.
23. Boland K, Flanagan L, Prehn JH. Paracrine control of tissue regeneration and cell proliferation by caspase-3. Cell Death Dis 2013;4:e725.
24. Huang Q, Li F, Liu X, Li W, Shi W, Liu FF, O'Sullivan B, He Z, Peng Y, Tan AC, et al. Caspase 3-mediated stimulation of tumor cell repopulation during cancer radiotherapy. Nat Med 2011;17:860–866.
25. O'Donovan N, Crown J, Stunell H, Hill AD, McDermott E, O'Higgins N, Duffy MJ. Caspase 3 in breast cancer. Clin Cancer Res 2003;9:738–742.
26. Janzen V, Fleming HE, Riedt T, Karlsson G, Riese MJ, Lo Celso C, Reynolds G, Milne CD, Paige CJ, Karlsson S, et al. Hematopoietic stem cell responsiveness to exogenous signals is limited by caspase-3. Cell Stem Cell 2008;2:584–594.
27. Suzuki M, Ito Y, Sakata I, Sakai T, Husimi Y, Douglas KT. Caspase-3 sensitive signaling in vivo in apoptotic HeLa cells by chemically engineered intramolecular fluorescence resonance energy transfer mutants of green fluorescent protein. Biochem Biophys Res Commun 2005;330:454–460.
28. Suzuki M, Tanaka S, Ito Y, Inoue M, Sakai T, Nishigaki K. Simple and tunable Förster resonance energy transfer-based bioprobes for high-throughput monitoring of caspase-3 activation in living cells by using flow cytometry. Biochim Biophys Acta 2012;1823:215–226.
29. Suzuki M, Sakata I, Sakai T, Tomioka H, Nishigaki K, Tramier M, Coppey-Moisan M. A high-throughput direct fluorescence resonance energy transfer-based assay for analyzing apoptotic proteases using flow cytometry and fluorescence lifetime measurements. Anal Biochem 2015;491:10–17.
30. Periasamy A. Fluorescence resonance energy transfer microscopy: A mini review. J Biomed Opt 2001;6:287–291.
31. Berney C, Danuser G. FRET or no FRET: a quantitative comparison. Biophys J 2003;84:3992–4010.
32. Gates EM, LaCroix AS, Rothenberg KE, Hoffman BD. Improving quality, reproducibility, and usability of FRET-based tension sensors. Cytometry A 2019;95:201–213.
33. Dumas JP, Jiang JY, Gates EM, Hoffman BD, Pierce MC, Boustany NN. FRET efficiency measurement in a molecular tension probe with a low-cost frequency-domain fluorescence lifetime imaging microscope. J Biomed Opt 2019;24:1–11.
34. Nagy P, Vereb G, Damjanovich S, Mátyus L, Szöllõsi J. Measuring FRET in flow cytometry and microscopy. Curr Protoc Cytom 2006; Chapter 12: Unit 12.8.
35. Sambrano J, Chigaev A, Nichani KS, Smagley Y, Sklar LA, Houston JP. Evaluating integrin activation with time-resolved flow cytometry. J Biomed Opt 2018;23:1–10.
36. Sands B, Jenkins P, Peria WJ, Naivar M, Houston JP, Brent R. Measuring and sorting cell populations expressing Isospectral fluorescent proteins with different fluorescence lifetimes. PLoS One 2014;9:e109940.
37. Li W, Vacca G, Castillo M, Houston KD, Houston JP. Fluorescence lifetime excitation cytometry by kinetic dithering. Electrophoresis 2014;35:1846–1854.

Caspase-3 in Fluorescence Lifetime-Based Cytometry Measurements and Phasor Analyses

38. Jenkins P, Naivar MA, Houston JP. Toward the measurement of multiple fluorescence lifetimes in flow cytometry: Maximizing multi-harmonic content from cells and microspheres. J Biophotonics 2015;8:908–917.

39. Alturkistany F, Nichani K, Houston KD, Houston JP. Fluorescence lifetime shifts of NAD(P)H during apoptosis measured by time-resolved flow cytometry. Cytometry A 2019;95:70–79.

40. Mitchell FL, Frank F, Marks GE, Suzuki M, Douglas KT, Bryce RA. Molecular dynamics study of chemically engineered green fluorescent protein mutants: Comparison of intramolecular fluorescence resonance energy transfer rate. Proteins 2009;75:28–39.

41. Tao W, Rubart M, Ryan J, Xiao X, Qiao C, Hato T, Davidson MW, Dunn KW, Day RN. A practical method for monitoring FRET-based biosensors in living animals using two-photon microscopy. Am J Physiol Cell Physiol 2015;309:C724–C735.

42. Shrestha D, Jenei A, Nagy P, Vereb G, Szöllősi J. Understanding FRET as a research tool for cellular studies. Int J Mol Sci 2015;16:6718–6756.

43. Liao JY, Song Y, Liu Y. A new trend to determine biochemical parameters by quantitative FRET assays. Acta Pharmacol Sin 2015;36:1408–1415.

44. Cao R, Jenkins P, Peria W, Sands B, Naivar M, Brent R, Houston JP. Phasor plotting with frequency-domain flow cytometry. Opt Express 2016;24:14596–14607.

45. Redford GI, Clegg RM. Polar plot representation for frequency-domain analysis of fluorescence lifetimes. J Fluoresc 2005;15:805–815.

46. Sands B, Jenkins P, Peria WJ, Naivar M, Houston JP, Brent R. Measuring and sorting cell populations expressing Isospectral fluorescent proteins with different fluorescence lifetimes. PLoS One 2014;9:e109940.

47. Martelo L, Fedorov A, Berberan-Santos MN. Fluorescence Pphasor plots using time domain data: Effect of the instrument response function. J Phys Chem B 2015;119:10267–10274.

48. Esposito A, Gerritsen HC, Oggier T, Lustenberger F, Wouters FS. Innovating lifetime microscopy: A compact and simple tool for life sciences, screening, and diagnostics. J Biomed Opt 2006;11:34016.

49. Houston JP, Yang Z, Sambrano J, Li W, Nichani K, Vacca G. Overview of fluorescence lifetime measurements in flow cytometry. Methods Mol Biol 2018;1678:421–446.

50. Sun Y, Day RN, Periasamy A. Investigating protein-protein interactions in living cells using fluorescence lifetime imaging microscopy. Nat Protoc 2011;6:1324–1340.

51. Silberberg M, Grecco HE. pawFLIM: Reducing bias and uncertainty to enable lower photon count in FLIM experiments. Methods Appl Fluoresc 2017;5:024016.

52. Digman MA, Caiolfa VR, Zamai M, Gratton E. The phasor approach to fluorescence lifetime imaging analysis. Biophys J 2008;94:L14–L16.

53. Hinde E, Digman MA, Hahn KM, Gratton E. Millisecond spatiotemporal dynamics of FRET biosensors by the pair correlation function and the phasor approach to FLIM. Proc Natl Acad Sci USA 2013;110:135–140.

54. Verveer PJ, Bastiaens PI. Evaluation of global analysis algorithms for single frequency fluorescence lifetime imaging microscopy data. J Microsc 2003;209:1–7.

55. Hanley QS, Clayton AH. AB-plot assisted determination of fluorophore mixtures in a fluorescence lifetime microscope using spectra or quenchers. J Microsc 2005;218:62–67.

56. Suzuki M, Ito Y, Savage HE, Husimi Y, Douglas KT. Protease-sensitive signalling by chemically engineered intramolecular fluorescent resonance energy transfer mutants of green fluorescent protein. Biochim Biophys Acta 2004;1679:222–229.

57. Suzuki M, Ito Y, Savage H, Husimi Y, Douglas K. Intramolecular fluorescent resonance energy transfer (FRET) by BODIPY chemical modification of cysteine-engineered mutants of green fluorescent protein. Chem Lett 2003;32:306–307.

58. Trón L, Szöllósi J, Damjanovich S, Helliwell SH, Arndt-Jovin DJ, Jovin TM. Flow cytometric measurement of fluorescence resonance energy transfer on cell surfaces. Quantitative evaluation of the transfer efficiency on a cell-by-cell basis. Biophys J 1984;45:939–946.

59. Houston JP, Naivar MA, Freyer JP. Digital analysis and sorting of fluorescence lifetime by flow cytometry. Cytometry A 2010;77:861–872.

60. Vermes I, Haanen C, Steffens-Nakken H, Reutelingsperger C. A novel assay for apoptosis. Flow cytometric detection of phosphatidylserine expression on early apoptotic cells using fluorescein labelled annexin V. J Immunol Methods 1995;184:39–51.

61. Heikal AA, Hess ST, Webb WW. Multiphoton molecular spectroscopy and excited-state dynamics of enhanced green fluorescent protein (EGFP): Acid–base specificity. Chem Phys 2001;274:37–55.

62. Hinde E, Digman MA, Welch C, Hahn KM, Gratton E. Biosensor Förster resonance energy transfer detection by the phasor approach to fluorescence lifetime imaging microscopy. Microsc Res Tech 2012;75:271–281.

63. Galluzzi L, Joza N, Tasdemir E, Maiuri MC, Hengartner M, Abrams JM, Tavernarakis N, Penninger J, Madeo F, Kroemer G. No death without life: Vital functions of apoptotic effectors. Cell Death Differ 2008;15:1113–1123.

64. D'Arcy MS. Cell death: A review of the major forms of apoptosis, necrosis and autophagy. Cell Biol Int 2019;43:582–592.